Analysis of Dynamics of Excitation and Dephasing of Plasmon Resonance Modes in Nanoparticles

I. D. Mayergoyz,[1] Z. Zhang,[1] and G. Miano[2]

[1]*Department of Electrical and Computer Engineering, Institute for Advanced Computer Studies, University of Maryland, College Park, Maryland, 20742, USA*

[2]*Department of Electrical Engineering, University of Naples Federico II, Via Claudio 21, Naples, I-80125, Italy*

(Received 29 September 2006; published 2 April 2007)

A novel theoretical approach to the dynamics analysis of excitation and dephasing of plasmon modes in nanoparticles is presented. This approach is based on the biorthogonal plasmon mode expansion, and it leads to the predictions of time dynamics of excitation of specific plasmon modes as well as their steady state amplitude and their decay. Temporal characteristics of plasmon modes in nanoparticles are expressed in terms of their shapes, permittivity dispersion relations, and excitation conditions. In the case of the Drude model, analytical expressions for time-dynamics of plasmon modes are obtained.

DOI: 10.1103/PhysRevLett.98.147401 PACS numbers: 78.67.Bf, 41.20.Cv, 42.25.Fx, 42.68.Mj

Plasmon resonances in nanoparticles have been the focus of considerable experimental and theoretical research lately. This research is motivated by numerous scientific and technological applications of these resonances in such areas as near-field microscopy, nanolithography, surface enhanced Raman scattering, nanophotonics, biosensors, optical data storage, etc. Steady state properties of plasmon resonances in nanoparticles have been mostly studied, while the dynamics of specific plasmon modes is the least understood area of plasmonics. This state of affairs has prompted the current burst of activity in the experimental research of plasmon dynamics. This research is exemplified by publications [1–6], where the plasmon dynamics and plasmon decay (dephasing) rates have been extensively studied by using advanced femtosecond techniques. The theoretical temporal analysis of plasmon modes is also very important to fully comprehend the time-dynamics of mode excitation and decay as well as to estimate their steady state amplitude. The temporal analysis of plasmon resonance modes can be very instrumental in the area of light controllability of plasmon resonances in semiconductor nanoparticles [7,8], where proper time synchronizations of excitations of specific plasmon modes may be needed.

In this Letter, we present a self-consistent theoretical technique for the temporal analysis of specific plasmon modes in nanoparticles and compare (where it is possible) the theoretical results with experimental data. This technique is based on the biorthogonal plasmon mode expansion, and it leads to the predictions of time-dynamics of excitation of specific plasmon modes and their decay as well as their steady state amplitude in terms of nanoparticle shapes, permittivity dispersion relations, and excitation conditions. For instance, an explicit formula is derived for the steady state amplitude of plasmon modes in terms of real and imaginary parts of dielectric permittivity, amplitude of incident field, and its spatial orientation with respect to dipole moments of the plasmon modes. In the case of the Drude model, analytical expressions for plasmon dynamics are obtained which suggest that the reciprocal of the Drude damping factor can be identified with the decay (dephasing) time of plasmon modes.

To start the discussion, consider a nanoparticle with boundary S and dielectric permittivity $\epsilon(\omega)$ in free-space with dielectric constant ϵ_0. It has been demonstrated [7–10] that the resonance values ϵ_k of dielectric permittivity and corresponding resonant plasmon modes can be found by solving the eigenvalue problems for the boundary integral equation

$$\sigma_k(Q) = \frac{\lambda_k}{2\pi} \oint_S \sigma_k(M) \frac{\mathbf{r}_{MQ} \cdot \mathbf{n}_Q}{r_{MQ}^3} dS_M, \tag{1}$$

or its adjoint equation

$$\tau_k(Q) = \frac{\lambda_k}{2\pi} \oint_S \tau_k(M) \frac{\mathbf{r}_{QM} \cdot \mathbf{n}_M}{r_{QM}^3} dS_M, \tag{2}$$

where $\sigma_k(M)$ has the physical meaning of surface electric charges on S that produce electric field $\mathbf{E}_k$ of k-th plasmon mode, $\tau_k(M)$ has the physical meaning of dipole densities on S that produce displacement field $\mathbf{D}_k$ of k-th plasmon mode, while all other notations have their usual meaning. The resonance values of ϵ_k and λ_k are related by

$$\lambda_k = \frac{\epsilon_k - \epsilon_0}{\epsilon_k + \epsilon_0}. \tag{3}$$

After λ_k are computed and resonance values of permittivity ϵ_k are found by using (3), resonance frequencies are determined from the dispersion relation:

$$\epsilon_k = \epsilon'(\omega_k) = \mathrm{Re}[\epsilon(\omega_k)]. \tag{4}$$

It turns out that eigenfunctions $\sigma_k(M)$ and $\tau_i(M)$ are biorthogonal:

$$\oint_S \sigma_k(M)\tau_i(M)dS_M = \delta_{ki}. \tag{5}$$

Thus, the set of eigenfunctions $\sigma_k(M)$ can be used for the biorthogonal expansion of actual boundary charges $\sigma(M, t)$ induced on particle boundary during the excitation process:

$$\sigma(M, t) = \sum_{k=1}^{\infty} a_k(t)\sigma_k(M), \tag{6}$$

where, according to (5), the expansion coefficient $a_k(t)$ is given by the formula

$$a_k(t) = \oint_S \sigma(M, t)\tau_k(M)dS_M. \tag{7}$$

It is clear that the time evolution of the expansion coefficient $a_k(t)$ reveals the time-dynamics of k-th plasmon mode corresponding to the eigenfunction $\sigma_k(M)$. Since the medium of resonant nanoparticle is dispersive and exhibits nonlocal in time constitutive relation $\mathbf{D}(t)$ vs $\mathbf{E}(t)$, the frequency domain technique will be employed for the calculations of $a_k(t)$. This means that the Eq. (6) and (7) will be Fourier transformed

$$\tilde{\sigma}(M, \omega) = \sum_{k=1}^{\infty} \tilde{a}_k(\omega)\sigma_k(M), \tag{8}$$

$$\tilde{a}_k(\omega) = \oint_S \tilde{\sigma}(M, \omega)\tau_k(M)dS_M, \tag{9}$$

and the equation for $\tilde{a}_k(\omega)$ will be first derived and solved. Subsequently, $a_k(t)$ will be found through inverse Fourier transform.

To derive the equation for $\tilde{a}_k(\omega)$, the Fourier transformed boundary condition for the normal components of electric field on S is invoked:

$$\epsilon(\omega)\tilde{E}_n^+(Q, \omega) - \epsilon_0\tilde{E}_n^-(Q, \omega) = [\epsilon_0 - \epsilon(\omega)]\tilde{E}_n^{(0)}(Q, \omega). \tag{10}$$

Here, $\tilde{E}_n^+(Q, \omega)$ and $\tilde{E}_n^-(Q, \omega)$ are the limiting values of the normal components of Fourier transformed electric field at $Q \in S$ from inside and outside S, respectively, while $\tilde{E}_n^{(0)}(Q, \omega)$ is the Fourier transformed normal component of the incident field on S.

By using formula $\tilde{\sigma}(Q, \omega) = \epsilon_0[\tilde{E}_n^-(Q, \omega) - \tilde{E}_n^+(Q, \omega)]$, the boundary condition (10) can be rearranged as follows:

$$\frac{\tilde{\sigma}(Q, \omega)}{\epsilon(\omega) - \epsilon_0} - \tilde{E}_n^+(Q, \omega) = \tilde{E}_n^{(0)}(\omega). \tag{11}$$

Now it can be recalled [11,12] that

$$\tilde{E}_n^+(Q, \omega) = -\frac{\tilde{\sigma}(Q, \omega)}{2\epsilon_0} + \frac{1}{4\pi\epsilon_0}\oint_S \tilde{\sigma}(Q, \omega)\frac{\mathbf{r}_{MQ}\cdot\mathbf{n}_Q}{r_{MQ}^3}dS_M. \tag{12}$$

By substituting (12) into (11) and then by using expansion (8) and formulas (1) and (9), the following expression for $\tilde{a}_k(\omega)$ is derived:

$$\tilde{a}_k(\omega) = \frac{2\epsilon_0\lambda_k[\epsilon(\omega) - \epsilon_0]}{2\epsilon_0\lambda_k + [\epsilon(\omega) - \epsilon_0](\lambda_k - 1)} \times \oint_S \tilde{E}_n^{(0)}(Q, \omega)\tau_k(Q)dS_Q. \tag{13}$$

The last integral can be simplified because the incident field $\mathbf{E}^{(0)}(Q, t)$ is practically uniform within nanoparticles. Thus, this field can be represented as $\mathbf{E}^{(0)}(Q, t) = \mathbf{E}_0 f(t)$. By using this form of $\mathbf{E}^{(0)}(Q, t)$ in (13) and taking into account formula (3) and the fact that due to the "scaling" freedom provided by normalization condition (5) the following expression $\oint_S \mathbf{n}_Q\tau_k(Q)dS_Q = (\epsilon_k - \epsilon_0)\mathbf{p}_k$ for the dipole moment $\mathbf{p}_k$ of k-th plasmon mode (see [8]) can be used, the last formula can be represented in the form

$$\tilde{a}_k(\omega) = (\mathbf{E}_0\cdot\mathbf{p}_k)\tilde{g}_k(\omega)\tilde{f}(\omega), \tag{14}$$

where

$$\tilde{g}_k(\omega) = \frac{\epsilon(\omega) - \epsilon_0}{\epsilon_k - \epsilon(\omega)}, \tag{15}$$

and $\tilde{f}(\omega)$ is the Fourier transform of $f(t)$.

Formulas (14) and (15) are remarkably simple, and they clearly suggest that $\tilde{g}_k(\omega)$ can be construed as normalized (by $\mathbf{E}_0\cdot\mathbf{p}_k$) transfer function of k-th plasmon mode. The formula (15) reveals the resonance nature of excitation of k-th plasmon mode at the frequency ω_k. Indeed, according to (4), at this frequency $\epsilon_k - \epsilon(\omega_k) = -i\mathrm{Im}[\epsilon(\omega_k)]$ and the magnitude of $\tilde{g}_k(\omega)$ will be narrow peaked if $\epsilon''(\omega_k)$ is sufficiently small, that is when the specific plasmon resonance is strongly pronounced.

By using formula (14), the following expression is derived for $a_k(t)$:

$$a_k(t) = (\mathbf{E}_0\cdot\mathbf{p}_k)\int_0^t g_k(t - t')f(t')dt', \tag{16}$$

with $g_k(t)$ being the inverse Fourier transform of $\tilde{g}_k(\omega)$. Thus, the algorithm of analysis of time-dynamics of k-th plasmon mode can be stated as follows. First, the eigenvalue problem (1) and (3) is solved and resonance values ϵ_k of dielectric permittivity and surface electric charges $\sigma_k(M)$ of the corresponding plasmon mode are found. Next, by using $\sigma_k(M)$, the dipole moment $\mathbf{p}_k$ is computed. Then, $g_k(t)$ is determined through the inverse Fourier transform of $\tilde{g}_k(\omega)$ given by (14). Finally, formula (16) is employed to evaluate the time evolution of $a_k(t)$ which reveals the time-dynamics of k-th plasmon mode. It is worthwhile to mention that the outlined computations can be performed by using actual, experimentally measured $\epsilon(\omega)$.

Expressions (14)–(16) can be useful for analytical calculations as well. To demonstrate this, consider the steady state case when $f(t) = \sin\omega_k t$, where ω_k is the resonance frequency defined by the formula (4). Then, $\tilde{f}(\omega) = i\sqrt{\frac{\pi}{2}}[\delta(\omega - \omega_k) - \delta(\omega + \omega_k)]$ and, by using (14) and

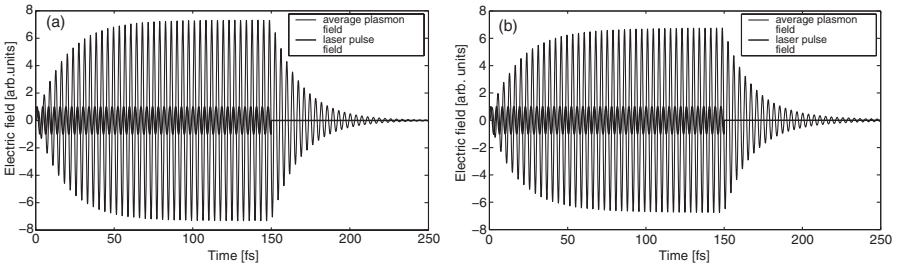

FIG. 1. Dynamics of plasmon resonances for Au nanorings (height 60 nm, inner radius 55 nm, outer radius 65 nm) on a glass substrate ($\epsilon_s = 2.25$) computed for the resonance wavelength 1102 nm (see [15]) by using (a) Drude model ($\gamma = 1.0753 \times 10^{14}$ s^{-1} [13]) and (b) Au dispersion relation from [13].

(15) as well as the inverse Fourier transform of $\tilde{a}_k(\omega)$, we arrive at

$$a_k^{(\mathrm{ss})}(t) = -(\mathbf{E}_0 \cdot \mathbf{p}_k)\left[\frac{\epsilon'(\omega_k) - \epsilon_0}{\epsilon''(\omega_k)}\cos\omega_k t + \sin\omega_k t\right], \quad (17)$$

where superscript (ss) indicates the steady state of $a_k(t)$.

In the case of strong plasmon resonances when $|\epsilon'(\omega_k) - \epsilon_0| \gg |\epsilon''(\omega_k)|$, the last formula is simplified as follows:

$$a_k^{(\mathrm{ss})}(t) = -(\mathbf{E}_0 \cdot \mathbf{p}_k)\frac{\epsilon'(\omega_k) - \epsilon_0}{\epsilon''(\omega_k)}\cos\omega_k t. \quad (18)$$

As typical for most resonances, the steady state is shifted by almost 90° in time with respect to the incident field $\mathbf{E}_0(t)$. It is also natural that the magnitude of the steady state is controlled by the ratio of real and imaginary parts of dielectric permittivity at the resonance frequency. It is also revealing that the resonance magnitude depends on the spatial orientation of the incident field $\mathbf{E}_0(t)$ with respect to the dipole moment $\mathbf{p}_k$ of plasmon resonance mode.

For off-resonance excitation $f(t) = \sin\omega_0 t$, similar calculations lead to the expression

$$a_k^{(\mathrm{ss})}(t) = (\mathbf{E}_0 \cdot \mathbf{p}_k)C(\omega_0)\cos(\omega_0 t + \varphi), \quad (19)$$

where

$$C(\omega_0) = \sqrt{\frac{[\epsilon'(\omega_0) - \epsilon_0]^2 + [\epsilon''(\omega_0)]^2}{[\epsilon_k - \epsilon'(\omega_0)]^2 + [\epsilon''(\omega_0)]^2}}. \quad (20)$$

Equation (20) is very instrumental for evaluations of the width of plasmon resonances.

Next, we point out that simple analytical expressions for $g_k(t)$ in (16) can be obtained for the Drude model of $\epsilon(\omega)$:

$$\epsilon(\omega) = \epsilon_0\left[1 - \frac{\omega_p^2}{\omega(\omega + i\gamma)}\right]. \quad (21)$$

Indeed, by using (21) in (15), we obtain

$$\tilde{g}_k(\omega) = -\frac{\omega_k^2 + \gamma^2}{(i\omega - \alpha_1)(i\omega - \alpha_2)}, \quad (22)$$

where $\alpha_1 = \frac{\gamma}{2} + i\beta$ and $\alpha_2 = \frac{\gamma}{2} - i\beta$, $\beta = \frac{\sqrt{4\omega_k^2 + 3\gamma^2}}{2}$. Now the inverse Fourier transform of (22) yields for $t > 0$

$$g_k(t) = -\frac{2(\omega_k^2 + \gamma^2)}{\sqrt{4\omega_k^2 + 3\gamma^2}}e^{-(\gamma/2)t}\sin\beta t. \quad (23)$$

Formulas (16) and (23) can be used for analytical calculations of $a_k(t)$ for "rectangular" laser pulses $\mathbf{E}^{(0)}f(t)$. Indeed, in the case when

$$f(t) = \begin{cases} 0 & \text{for } t < 0, \\ \sin\omega_k t & \text{for } t \geq 0, \end{cases} \quad (24)$$

from (16), (23), and (24), we derive

$$a_k(t) = -(\mathbf{E}_0 \cdot \mathbf{p}_k)\omega_k e^{-(\gamma/2)t}\left(\frac{1}{\gamma}\cos\beta t - \frac{2}{\beta}\sin\beta t\right) + a_k^{(\mathrm{ss})}(t), \quad (25)$$

where

$$a_k^{(\mathrm{ss})}(t) = (\mathbf{E}_0 \cdot \mathbf{p}_k)\left(\frac{\omega_k}{\gamma}\cos\omega_k t - \sin\omega_k t\right). \quad (26)$$

In the case of finite rectangular laser pulse $f(t) = \sin\omega_k t$, $T \leq t \leq 0$, from (16) and (23) we derive for $t > T$

$$a_k(t) = -(\mathbf{E}_0 \cdot \mathbf{p}_k)e^{-(\gamma/2)(t-T)}\left[\omega_k e^{-(\gamma/2)T}\left(\frac{1}{\gamma}\cos\beta t - \frac{2}{\beta}\sin\beta t\right) - \left(\frac{\omega_k}{\gamma}\cos\omega_k t - \sin\omega_k t\right)\right]. \quad (27)$$

It is instructive to compare the computational results obtained by using the Drude model with those obtained by using the experimentally measured dispersion relation

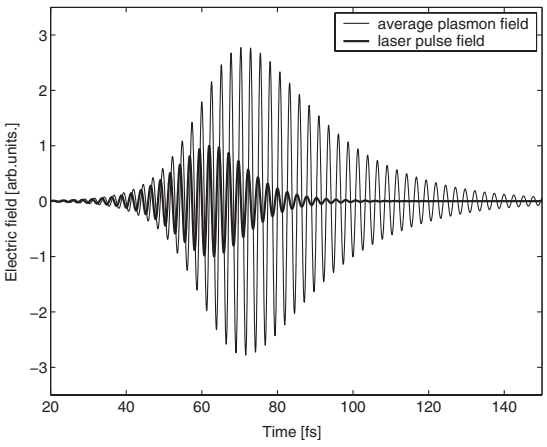

FIG. 2. Dynamics of plasmon resonances for Au cylinders (height 14 nm, diameter 126 nm) on a glass substrate ($\epsilon_s = 2.25$) computed for the resonance wavelength 774 nm (see [2]). The Au dispersion relation from [13] have been used in computations.

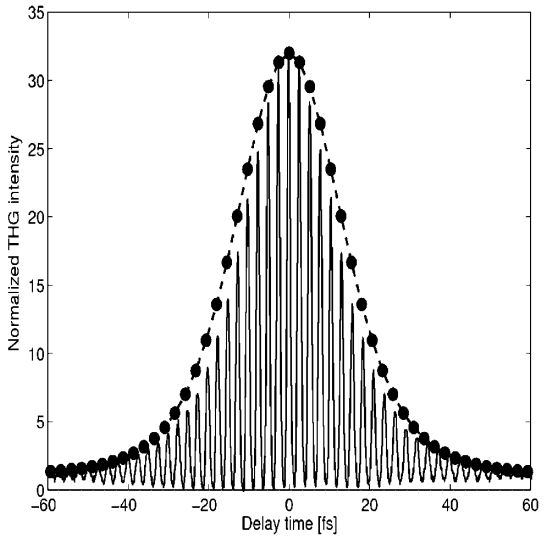

FIG. 3. Envelop of the calculated third order ACF (filled circles) superimpose on the measured third order ACF (solid line) from [2] for Au cylinders on a glass substrate at wavelength 774 nm (maximum is normalized to 32).

$\epsilon(\omega)$. This comparison is presented by Figs. 1(a) and 1(b) for Au rings subject to finite rectangular laser pulses. These figures suggest that the Drude model leads to quantitatively similar results as the use of actual dispersion relation. Formula (27) also implies that $1/\gamma$ can be identified as the decay (dephasing) time for the light intensity of plasmon modes. In accordance with the available data for γ (see [13,14]), this suggests that formula (27) predicts the decay (dephasing) time for plasmon modes in gold (and silver) nanoparticles in the range of 5–12 fs, which is consistent with the experimental results reported in [1–6,14].

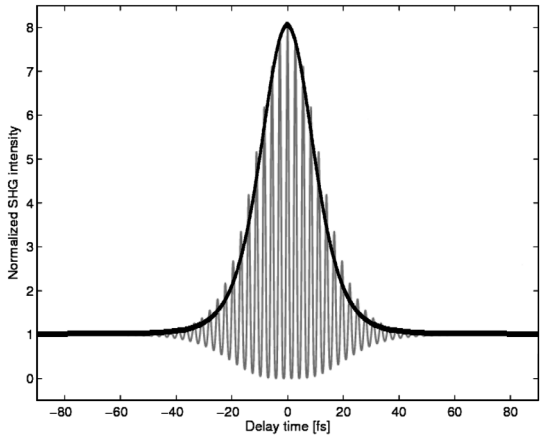

FIG. 4. The calculated second-order ACF superimpose on the envelop of measured second-order ACF from [6] for noncentrosymmetric L-shape Au nanoparticles (height 21 nm, arm length 150 nm, arm width 75 nm) on a tantalum-dioxide substrate ($\epsilon_s = 4.33$) at wavelength 838 nm (maximum is normalized to 8).

Finally, we present the comparison between computational results based on the technique outlined above and experimental results presented in [2,6]. By using Eqs. (15) and (16) we have computed the time-dynamics of the 774 nm resonance wavelength plasmon mode for Au cylinders on glass substrate [2]. Figure 2 presents the time variation of the incident electric field of the laser pulse (bold line) used in experiments reported in [2] and the corresponding computed time-dynamics of the average (over nanoparticle volume) electric field of the plasmon mode (thin line). The computed plasmon time-dynamics was used to compute the third order autocorrelation function (ACF) which was compared with the experimentally measured ACF from [2]. The results of this comparison are presented in Fig. 3. Figure 4 presents the comparison between our calculations of the second-order ACF for noncentrosymmetric L-shape gold nanoparticles from [6] and the experimentally measured in [6] second-order ACF. Figures 3 and 4 suggest the agreement with experimental data within 10%.

[1] B. Lamprecht, A. Leiner, and F. R. Aussenegg, Appl. Phys. B **64**, 269 (1997).
[2] B. Lamprecht, J. R. Krenn, A. Leitner, and F. R. Aussenegg, Phys. Rev. Lett. **83**, 4421 (1999).
[3] J. Lehmann, M. Merschdorf, W. Pfeiffer, A. Thon, S. Voll, and G. Gerber, Phys. Rev. Lett. **85**, 2921 (2000).
[4] A. Kubo, K. Onda, H. Petek, Z. Sun, Y. S. Jung, and H. K. Kim, Nano Lett. **5**, 1123 (2005).
[5] O. L. Muskens, N. D. Fatti, and F. Vallee, Nano Lett. **6**, 552 (2006).
[6] T. Zentgraf, A. Christ, J. Kuhl, and H. Giessen, Phys. Rev. Lett. **93**, 243901 (2004).
[7] D. R. Fredkin and I. D. Mayergoyz, Phys. Rev. Lett. **91**, 253902 (2003).
[8] I. D. Mayergoyz, D. R. Fredkin, and Z. Zhang, Phys. Rev. B **72**, 155412 (2005).
[9] F. Ouyang and M. Isaacson, Philos. Mag. B **60**, 481 (1989).
[10] F. Ouyang and M. Isaacson, Ultramicroscopy **31**, 345 (1989).
[11] O. D. Kellogg, *Foundation of Potential Theory* (McGraw-Hill, New York, 1929).
[12] S. G. Mikhlin, *Mathematical Physics, an Advanced Course* (North-Holland, Amsterdam, 1970).
[13] P. B. Johnson and R. W. Christy, Phys. Rev. B **6**, 4370 (1972).
[14] G. Gay, O. Alloschery, B. Viaris De Lesegno, C. O'dwyer, J. Weiner, and H. J. Lezec, Nature Phys. **2**, 262 (2006).
[15] J. Aizpurua, P. Hanarp, D. S. Sutherland, M. Kall, G. W. Bryant, and F. J. Garciade Abajo, Phys. Rev. Lett. **90**, 057401 (2003).